MATERIALS CHEMISTRY FRONTIERS

CCS 中国化学会 CHINESE CHEMICAL SOCIETY

ICCAS

ROYAL SOCIETY OF CHEMISTRY

The Role of Dipole Moment in Two Fused-Ring Electron Acceptors with One Polymer Donor based Ternary Organic Solar Cells

Journal:	*Materials Chemistry Frontiers*
Manuscript ID	QM-RES-01-2020-000016.R1
Article Type:	Research Article
Date Submitted by the Author:	24-Mar-2020

Complete List of Authors:	Liao, Xunfan; Donghua University, Materials Science and Engineering Cui, Yongjie; Donghua University shi, xueliang; East China Normal University, School of Chemistry and Molecular Engineering Yao, Zhaoyang; KTH Royal Institute of Technology, Zhao, Heng; Xi'an Jiaotong University, State Key Laboratory for Mechanical Behavior of Materials An, Yongkang; Nanchang University Zhu, Peipei; Nanchang University Guo, Yaxiao; KTH Royal Institute of Technology Fei, Xiang; Donghua University, College of Material Science and Engineering Zuo, Lijian; University of Washington, Materials Science and Engineering; employer Gao, Ke; University of Washington College of the Environment, Lin, Francis; University of Washington, Department of Chemistry Xie, Qian; Nanchang University, College of Chemistry/Institute of Polymers Chen, Lie; Nanchang University, College of Chemistry/Institute of Polymers Ma, Wei; Xi'an Jiaotong University, State Key Laboratory for Mechanical Behavior of Materials Chen, Yiwang; Nanchang University, College of Chemistry Jen, Alex; University of Washington, Materials Science and Engineering; University of Washington, Chemistry

ARTICLE

The Role of Dipole Moment in Two Fused-Ring Electron Acceptors with One Polymer Donor based Ternary Organic Solar Cells

Received 00th January 20xx,
Accepted 00th January 20xx

DOI: 10.1039/x0xx00000x

Xunfan Liao, ‡[a,b] Yongjie Cui, ‡[b] Xueliang Shi,*[,c] Zhaoyang Yao,[g] Heng Zhao,[f] Yongkang An,[h] Peipei Zhu,[a] Yaxiao Guo,[g] Xiang Fei,[b] Lijian Zuo,[d] Ke Gao,[d] Francis Lin,[d] Qian Xie,[h] Lie Chen,[h] Wei Ma,*[,f] Yiwang Chen,*[a] Alex K.-Y. Jen,*[,d,e]

Fused-ring electron acceptors (FREAs) based ternary organic solar cells (OSCs) have made significant progress and attracted considerable attention due to their simple device architecture and broad absorption range in devices. There are three key parameters that need to be fine-tuned in ternary OSCs including absorption, energy level and morphology in order to realize high efficiencies. Herein, a series of FREAs with diverse electron-rich cores or electron-deficient terminals are developed and rationally combined to achieve high performance ternary OSCs. A new factor of dipole moment of FREAs' terminals is unveiled and its working mechanism has been thoroughly investigated by systematical studying of six ternary OSCs. These ternary blends all exhibit complementary absorptions and cascade energy levels, which can facilitate efficient light-harvesting and charge transfer. Additionally, the morphological effects on ternary OSCs are eliminated through comparative studies while demonstrating distinctively different performance. The preliminary results show that compatible dipole moment between two FREAs is critical in ternary blends. Specifically, the performance of the ternary system with two FREAs having quite different dipole moment terminals is worse than that with similar terminal dipole moments. The pair with larger difference in dipole moment will also negatively impact device performance. This interesting phenomenon is likely due to that very different dipole moments of terminals in FREAs can significantly decrease the electron mobility as well as induce unbalanced hole/electron transport. Consequently, it results in increased charge recombination and reduced charge collection efficiency. This finding demonstrates that dipole moment of FREAs should be taken into account in designing ternary OSCs.

1. Introduction

Non-fullerene acceptors (NFAs) based organic solar cells (OSCs) have attracted great attention and significant progress have been made due to their broad absorption in both visible and near-infrared (NIR), easily adjustable energy levels, and tunable crystallinity in active layer morphology.[1-8] To achieve efficient OSCs, effective absorbing sun light from the active layer is very critical. Thus, considerable efforts have been devoted to the design of active layer materials and device structures to ensure broadened absorption.[9-19] For example, tandem solar cells by stacking multiple photoactive layers with complementary absorption spectra can capture more photon flux to improve short-circuit current density (J_{sc}).[20-24] Although a high power conversion efficiency (PCE) of 17.3% was obtained,[25] the application of tandem OSCs is still quite limited because of the complexity in device fabrication and large-scale production.

Compared with tandem OSCs, ternary solar cells where the active layer typically consists of either two donors and one acceptor or one donor and two acceptors have the simplicity of the single junction structure and broadened absorption of active layer.[26-30] However, there are three key parameters including absorption, energy level and morphology that need to be fine-tuned simultaneously in order to realize efficient device performance. Although the absorption and energy level of the third component can be easily determined by photophysical and electrochemical measurements for the ternary system, the morphology of ternary system is more difficult to control.[31-33] Recently, Yan et al. reported an effective method of minimizing interfacial tension between two fused-ring electron acceptors (FREAs) to control the morphology[34] of ternary system.[35-40] Although the PCE of this type of ternary OSCs has been significantly increased to over 16%,[41-44] a tedious trial-and-error approach involving the fabrication of large number of devices is often employed. Therefore, it would be highly desirable to develop a simple and intuitive method to effectively predict

[a] Institute of Advanced Scientific Research, Jiangxi Normal University, 99 Ziyang Avenue, Nanchang 330022, China. Email: ywchen@ncu.edu.cn
[b] State Key Laboratory for Modification of Chemical Fibers and Polymer Materials & College of Materials Science and En-gineering, Donghua University, Shanghai 201620, China.
[c] Shanghai Key Laboratory of Green Chemistry and Chemical Processes, School of Chemistry and Molecular Engineering, East China Normal University, Shanghai 200062, China. Email: xlshi@chem.ecnu.edu.cn
[d] Department of Materials Science and Engineering, University of Washington, Seattle, WA 98195 (USA). Email: ajen@uw.edu
[e] Department of Chemistry, City University of Hong Kong, Kowloon, Hong Kong.
[f] State Key Laboratory for Mechanical Behavior of Materials, Xi'an Jiaotong University, Xi'an 710049, China. Email: msewma@xjtu.edu.cn
[g] Department of Chemistry, Organic/Applied Physical Chemistry, KTH Royal Institute of Technology, Stockholm 10044, Sweden.
[h] Institute of Polymers and Energy Chemistry, College of Chemistry, Nanchang University, Nanchang 330031, China.
† Electronic Supplementary Information (ESI) available. See DOI: 10.1039/x0xx00000x.
‡ These authors contributed equally to this work.

what kind of FREA structures should be used in a ternary system.

It has been reported that charge separation and charge transfer involved in the FREAs based OSCs is very different from those of fullerene-based acceptors.[45] For the blend based on the single polymer donor and a fullerene acceptor, the ultrafast charge transfer originates from the variation in the π-electron densities of the donor and the acceptor. However, it is very different for the FREAs based blends such as those using ITIC derivatives. These kinds of acceptors usually have electron-rich cores with terminal electron-deficient groups such as substituted 3-(dicyanomethylidene)-indan-1-one (IC) and its fluorinated or chlorinated derivatives. Considering the strong electron withdrawing di-cyano-substituted terminals in FREAs, there may be some dipole effect from the terminals that can facilitate the charge transfer and at the same time prevent bimolecular recombination when these terminals are near the electron-rich polymer donor. Besides, recent crystallographic analysis revealed that terminal ICs form intermolecular π–π stacking with each other which might contribute to their efficient charge transfer.[18] Therefore, the terminal's dipole moment or the electronegativity of FREAs may play a vital role in facilitating charge separation and transfer in the binary blends.[46] Since there is no systematic investigation of these effects in FREA-based ternary OSCs, it is important to verify them and exploit the possibility of establishing a new material selection rule to expedite the development of this field.

In this work, we have developed a series of FREAs with different electron-rich cores or electron-deficient terminal groups and systematically studied them in six ternary blends to confirm the effect of 4TBA and 4TIC-4F have the largest difference in terminal dipole moment in ternary OSCs. As shown in **Scheme 1**, we initially use a polymer PBDT-2TC synthesized in house with suitable energy levels and intense absorption in the region between 400 and 650 nm as donor to match with these FREAs.[47] Two FREAs (4TBA and 6TBA) with similar donor core and the same terminals 1,3-diethyl-2-thioxodihydropyrimidine-4,6(1H, 5H)-dione (BA) are combined with polymer PBDT-2TC to form the first ternary blends PBDT-2TC:4TBA:6TBA. Then, the second and third ternary blends PBDT-2TC:4TBA:ITIC and PBDT-2TC:4TBA:4TIC are formed by combining 4TBA with ITIC and 4TIC, respectively. These FREAs have similar or same donor core but with different terminal groups. The results show that ternary blends based on acceptors with different terminals have worse device performance than those with the same terminals, especially the PBDT-2TC:4TBA:6TBA blend shows the best performance. The PBDT-2TC:4TBA:ITIC and PBDT-2TC:4TBA:4TIC devices have significantly lower electron mobility, which results in unbalanced hole/electron transport and increased charge recombination. These three ternary blends all exhibit complementary absorption and cascade energy levels, and the morphologies of these blend films are also quite similar. Therefore, there must be some other parameters that dictate the quite different performance of these ternary OSCs.

We then compare the terminals' dipole moment of these acceptors by DFT calculation. It shows the dipole moment value for the different terminals, Th-BA, Th-IC and Th-DFIC is gradually increased. To confirm our hypothesis, the acceptor 4TIC-4F with the same donor core 4T but has the largest dipole moment terminal 2-(5,6-difluoro-3-oxo-2,3-dihydro-1H-inden-1-ylidene)malononitrile (DFIC) was used to form the fourth ternary blend PBDT-2TC:4TBA:4TIC-4F. This blend only shows a little higher crystallinity than that of the binary blend while its electron mobility is the worst, leading to the most unbalanced uh/ue value and the poorest PCE. This result also reveals that larger dipole moment difference in FREAs will cause worse device performance.

To further verify the hypothesis and to exclude the interference from the donor core, another two ternary blends of PBDT-2TC:4TBA:STBA and PBDT-2TC:ITIC:4TIC with the same terminal but different donor cores were investigated as well. The novel acceptor, STBA was synthesized by connecting a novel donor core selenophene-thieno[3,2-b]thiophene-selenophene (ST) with the same terminal group, 4TBA. Although it has quite huge difference in the donor core, the performance of PBDT-2TC:4TBA:STBA blend shows small attenuation compared to that of the binary blend. The device of PBDT-2TC:ITIC:4TIC also works well with improved performance that can exclude the interference from the donor core. Therefore, the comparative studies of six ternary systems verify the importance of FREA dipole moment in choosing the suitable third component in ternary OSCs. Although this discovery may not be generally applicable to all systems, it does serve some guidance for further improving the performance of ternary OSCs.

2. Results and discussion

2.1. Ternary Blends Design and Quantum Calculations

The polymer donor employed in this work is PBDB-2TC (shown in **Scheme 1**), which has been previously reported by our group and showed good performance with FREAs.[47] As shown in **Scheme 1a**, three terminals, BA, IC and DFIC with different electronegativity are investigated, and their derived NIR FREAs such as 6TBA,[48] 4TIC[18], ITIC[1] and 4TIC-4F[49] are employed in this study. We have also developed another host acceptor 4TBA to evaluate the effects of different FREAs because it has matched energy level and complementary absorption with polymer PBDT-2TC and the above NIR FREAs. Four ternary blends PBDT-2TC:4TBA:6TBA, PBDT-2TC:4TBA:ITIC, PBDT-2TC:4TBA:4TIC and PBDT-2TC:4TBA:4TIC-4F are carefully designed to study these ternary OSCs. In addition, a novel acceptor STBA with ST as electron-rich core was also synthesized to systematically study the dipole moment effect in ternary OSCs by excluding the possible interference from the donor core.

4TBA and STBA were synthesized by Knoevenagel condensation reaction (**Scheme 1b**) and the synthetic de-tails and the related characterization are available in the Supporting Information (**Fig. S1-S4, ESI†**). Density function-al theory (DFT) calculations at the B3LYP/6-31G(d,p) level were used to calculate the highest occupied molecular orbital (HOMO) and the lowest unoccupied molecular orbital (LUMO) energies of the donor cores (IDTT, ST,

4T and ST), and the terminal groups (BA, IC and DFIC), in addition to the dipole moments of the terminal groups. As shown in **Fig. 1a**, both 4T, ST and 6T central cores have higher HOMO level than that of the IDTT, indicating their better electron-donating ability, which favors the NIR absorbing capability of FREAs. Regarding to terminal groups, BA's LUMO level is much higher than that of IC group, which is the highest among the four terminal groups, indicating its weakest electron-withdrawing ability. Compared to the IC group, fluorinated IC groups possess deeper LUMO level which agree with the reported values. The different electron-withdrawing ability of terminal groups deriving from their different electronegativity can be compared by calculating their regional dipole moments shown in **Fig. 1b**. Dipole moments of 4.166, 4.439, 4.884 and 5.420 D were observed for the Se-BA, T-BA, T-IC and T-DFIC segments, respectively. It is clear that the dipole moment of T-BA is significantly different from that of T-DFIC, which may induce unbalanced charge transport in two segments based binary acceptors (vide infra).

2.2. Electrochemical and Optical Properties

Absorption and energy level of the third component acceptor are widely considered to be crucial for efficient ternary OSCs. In order to eliminate the interference of these two factors and study the effect of electronegativity in ternary OSCs, six ternary blends with appropriate energy levels and complementary absorption are constructed (**Fig. 2**). The electrochemical properties of all these materials were investigated by cyclic voltammetry (CV) in the same condition (**Fig. 2a**, **Table S1** and **Figure S5, ESI†**). From the onset of oxidation potentials in the CV, the HOMO energy level of PBDT-2TC was determined to -5.37 eV, while its LUMO level was difficult to obtain from the CV measurement due to the unreliable reduction data. Thus, we used the optical bandgap and HOMO level to estimate the PBDT-2TC's LUMO level to be -3.41 eV. The HOMO/LUMO energy levels of the new acceptor 4TBA and STBA were estimated to be −5.51 eV/−3.70 eV and −5.45 eV/−3.60 eV, respectively. Similarly, the HOMO/LUMO energy levels of the 6TBA, ITIC, 4TIC and 4TIC-4F were estimated to be −5.41 eV/−3.66 eV, −5.60 eV/−3.86 eV, −5.56 eV/−4.03 eV and −5.60 eV/−4.21 eV, respectively.

Evidently, the first five ternary blends all exhibit cascade energy levels, which is believed to be beneficial for charge transfer. Notably, the sixth ternary blend shows multiple electron charge transfer, and nonradiative Förster resonance energy transfer (FRET) between the ITIC and 4TIC, which may improve the device performance. The normalized UV–vis absorption profiles of PBDT-2TC and FREAs in film state, and six ternary blends are shown in **Fig. 2b-g** and the absorption spectrum of the new acceptor 4TBA and STBA in dichloromethane solution are presented in **Fig. S6, ESI†**. From the UV-vis spectra, 4TBA exhibits strong absorption from 550 to 730 nm, which is expected to complement the absorption of PBDT-2TC. 4TBA film shows an absorption edge at 746 nm corresponding to an optical bandgap of 1.66 eV. Compared to 4TBA, STBA exhibits redshifted absorption (780 nm) and reduced bandgap (1.59 eV), which is ascribe to the more electron-rich ST unit and stronger intramolecular charge transfer of STBA. The third component 6TBA, ITIC, 4TIC and 4TIC-4F all show redshifted absorption com-pared to the host acceptor 4TBA, which can potentially benefit the absorption of the ternary blends. As a result, the six ternary blends all display complementary absorption, which is beneficial for light-harvesting. Thus, the potential interference from the factors (appropriate energy levels and complementary absorption) in the six selected ternary blends has been eliminated, which help study the effect of dipole moment in ternary OSCs.

2.3. Photovoltaic Device Performance

Ternary OSCs were fabricated in a conventional device configuration of ITO/PEDOT:PSS/PBDT-2TC:acceptor1:acceptor2/C60-bis/Ag, where C_{60}-bis is bis-fulleropyrrolidium iodide salt.[50] The molecular structure of C60-bis and the device structure are shown in **Fig. 3a** and **3b**, respectively. The acceptor 1 in this work is 4TBA and the binary BHJ device of PBDT-2TC:4TBA gave the best performance at the optimal condition of do-nor/acceptor weight ratio 1:1 in 1,2-dichlorobenzene (DCB) solution with thermal annealing at 120 °C for 10 min at 2000 rpm. The details for device optimization were shown in **Table S2** and **S3, ESI†**. Then, the weight ratio is kept at 1:1 (polymer:total acceptor) for all ternary blends with only the acceptors' relative weight ratio being tuned. We first optimized the ternary blend PBDT-2TC:4TBA:6TBA. As shown in **Table 1** and **Fig. 3c**, the binary device based on PBDT-2TC:4TBA exhibited a high V_{oc} of 0.962 V and FF of 0.71, delivering a high PCE of 10.52%. By varying the amount of 6TBA in ternary blends, the V_{oc} of the related devices increase while the Jsc and FF increase initially but then decease gradually. When the ratio of 4TBA:6TBA was 9:1, the highest PCE of 11.73% was obtained with a V_{oc} of 0.968 V, a J_{sc} of 16.6 mA cm^{-2}, and a FF of 0.73.

Next, the weight ratio is kept at 1:0.9:0.1 for other five ternary blends and all the other conditions of device fabrication kept consistent to perform a fair comparison on important device parameters. Then, a third component ITIC which has similar absorption range replaced 6TBA and constructed the ternary blend PBDT-2TC:4TBA:ITIC. Different to the previous ternary system, the Voc, Jsc and FF of the ternary blend device all dropped, leading to a decreased PCE of 8.73%. The decreased performance is due to the large difference between the donor core of ITIC and 4TBA. Based on this, 4TIC which has the same donor core with 4TBA and the same terminal group with ITIC was used to build another ternary OSCs. Similarly, we found that although the 4TIC absorption broadened and even redshifted to 900 nm, the device performance of PBDB-2TC:4TBA:4TIC is also significantly decreased (PCE decreased from 10.52% to 6.35%). More notably, the decreased is more pronounced (PCE decreased from 10.52% to 3.57%) when the fluorine atoms are introduced at the end of the 4TIC in PBDT-2TC:4TBA:4TIC-4F ternary system. Thus, we speculate that the large difference in the dipole moment between the two acceptors' terminal groups could affect the performance of the ternary OSCs.

To confirm the effect of dipole moment in ternary OSCs and exclude the interference of donor core, the performance of another two ternary blends of PBDT-2TC:4TBA:STBA and PBDT-

2TC:ITIC:4TIC with same terminal and different donor core were investigated. Although huge difference in the donor core, the PCE of PBDT-2TC:4TBA:STBA blend decreased little compared to the binary blend (PCE decreased from 10.52% to 9.51%). The device of PBDT-2TC:ITIC:4TIC work well and its PCE improved from 9.94% to 10.81%, as shown in **Table 1** and **Fig. S7, ESI†**. Therefore, from the results of the above six ternary OSCs, we can see the terminals' dipole moment of the combined acceptors have a more significant impact on device performance, especially for the key parameters FF and J_{sc}. The changed J_{sc} were confirmed by external quantum efficiency (EQE) measurements, as shown in **Fig. 3e** and **3f**. **Fig. 3e** displays the EQE curves of PBDT-2TC:4TBA:6TBA ternary devices with different acceptor ratios. PBDT-2TC:4TBA based binary device showed a high EQE response in the wavelength region of 350–750 nm. After the addition of 10% 6TBA, the EQE is broadened to 780 nm, which is consistent with the broadened absorption of 6TBA. **Fig. 3f** shows the EQE curves of the multiple ternary OSCs. It is clearly that the intensity of EQE response significantly decreased after the addition of ITIC, 4TIC and especially for 4TIC-4F. From integration of the EQE curves, the calculated Jsc was obtained, which are within reasonable difference to the J_{sc} values obtained from the corresponding *J*–*V* curves (**Table 1**).

2.4. Morphology Analysis

The morphology of the BHJ active layer plays a significant role on affecting the device performance. In order to differentiate if the performance of the above ternary OSCs is really affected by the acceptor terminal group's dipole moment or influenced by the BHJ morphology, we have carried out the grazing incidence wide-angle scattering (GIWAXS) measurements[51] on the samples studied above. GIWAXS can provide the information of molecular packing and crystalline orientation of these ternary BHJs. The GIWAXS 2D patterns and the corresponding line-cut profiles are shown in **Fig. 4** and **Fig. S8, ESI†**. It's obvious that all the binary and ternary films exhibit a face-on favorable orientation, as proven by the prominent (010) π–π stacking peaks in the out-of-plane direction.[52-53] For all ternary films, the addition of the third component didn't cause any significant change in morphology compared to those derived from binary PBDT-2TC:4TBA and PBDT-2TC:6TBA films. In addition, all the ternary films exhibit similar (100) lamellar stacking peaks at q ≈ 0.28 Å^{-1} in the in-plane direction and similar (010) π–π stacking peaks at q ≈ 1.65 Å^{-1} in the out-of-plane direction, suggesting that all the ternary films exhibit similar molecular packing and crystalline orientation. However, the device performance of these multiple ternary OSCs are quite different from each other. Therefore, the differences in performance among these ternary OSCs are not really caused by the morphology of the BHJ active layers.

2.5. The Role of Dipole Moment and Impact on Charge Transfer

To confirm the effect of the dipole moment on ternary OSCs and study the working mechanism, the steady state photoluminescence (PL) and time-resolved PL (TRPL) were performed. As shown in **Fig. 5a**, we first studied the effect of blend ratio on the charge transfer properties of PBDT-2TC:4TBA:6TBA ternary blend. The peak emission of pure PBDT-2TC film is located at 642 nm. For the blend films, the PL emission of PBDT-2TC is almost completely quenched and when the ternary blend (PBDT-2TC:4TBA:6TBA) weight ratio was 1:0.9:0.1, the PL peak is the most significantly quenched. Other ternary blends (shown in **Fig. 5b**) also exhibited the similar results, demonstrating that the photoexcited electrons could be efficiently transferred from the polymer donor to the acceptors. This result agrees well with previous literatures which reported that when FREAs' end groups approach the electron-enriched backbone of the polymer donor,[45] the strong dipole effect of the end groups may facilitate the charge transfer process.

Among these ternary blends, PBDT-2TC:4TBA:6TBA displayed the fastest exciton dissociation revealed by its shortest exciton lifetime (1.56 ns) which was fitted from the TPRL spectra (**Fig. 5c**). This favorable charge separation efficiency could also contribute to the higher J_{sc} and photovoltaic performance. In comparison, the ternary blend PBDT-2TC:4TBA:4TIC-4F showed the longest exciton lifetime of 3.87 ns, suggesting the slowest exciton dissociation in the active layer. It is very interesting that the speeds of exciton dissociation differ from each ternary blend while the difference in overall charge separation efficiency are similar (revealed by PL quenching efficiency, **Fig. 5b**). This indicates that dipole moment may have little effect on the processes of charge separation and transfer between donor and acceptor. It may have a stronger impact on the subsequent charge transport between the acceptors due to the electrons are transported along the acceptor materials.

To investigate the terminal's dipole moment on ternary OSCs' charge transport, the electron and hole mobilities of multiple ternary blend films were determined using the space-charge-limited-current method[54] with single-carrier device architectures of ITO/ZnO/Active layer/C_{60}-bis/Ag and ITO/PEDOT:PSS/Active layer/MoO_3/Ag), respectively. As shown in **Fig. 5d**, **Table 2** and **Fig. S9**, **ESI†** both the binary and multiple ternary devices exhibited high hole mobilties (u_h) with a small variation (1.56-1.99 × 10^{-4} cm^2 V^{-1} s^{-1}). Compared to the binary blend, both the hole mobilities for ternary blends PBDT-2TC:4TBA:6TBA, PBDT-2TC:4TBA:ITIC and PBDT-2TC:4TBA:4TIC were improved which may due to the increased crystallinity of the BHJ morphologies. Nevertheless, the electron mobilties (u_e) are strongly dependent on the difference of terminal's electronegativity between two FREAs in ternary blends. Compared to the u_e for binary blend (3.94 × 10^{-5} cm^2 V^{-1} s^{-1}), the u_e for the ternary blend PBDT-2TC:4TBA:4TIC-4F decreased dramatically to 3.89 × 10^{-6} cm^2 V^{-1} s^{-1}, leading to significantly unbalanced charge mobilities (u_h/u_e = 40.1), which is detrimental to charge transport and collection, and thus resulting in the low J_{sc} and FF values. For the ternary blends with two acceptors based on same terminals, the charge transport balance of u_h/u_e is 3.48 and 5.17 for PBDT-2TC:4TBA:6TBA and PBDT-2TC:4TBA:STBA, respectively. Meanwhile, for the ternary blends with two acceptors based on different terminals, the charge transport becomes more and more unbalanced (u_h/u_e = 6.03 for PBDT-2TC:4TBA:ITIC, u_h/u_e = 20.54 for PBDT-2TC:4TBA:4TIC), which could result in increased charge recombination (vide infra). These results demonstrate that the

terminals' dipole moment of acceptors could affect the charge transport and play an important role in ternary OSCs.

2.6. Recombination Analysis

To confirm that the unbalanced charge transport could result in increased charge recombination, we have studied the dependence of J_{sc} and V_{oc} on light intensity (I), as shown in **Fig. 5e** and ***5f***. In general, the relationship between J_{sc} and I follows a power-law formula of $Jsc \propto I^{\alpha}$, where the slope of the curve (α) reflects the bimolecular recombination degree and if α is closer to unity, suggesting the weak bimolecular recombination in active layers.[55-56] **Fig. 5e** depicts the plots of log J_{sc} versus log I, the α values are 0.96, 0.97 and 0.94 for the PBDT-2TC:4TBA binary device, PBDT-2TC:4TBA:6TBA and PBDT-2TC:4TBA:STBA ternary devices, respectively, implying less charge recombination loss during charge extraction in the PBDT-2TC:4TBA:6TBA devices. Clearly, in the ternary systems based on two acceptors with different terminals' dipole moment, the α values decreased to 0.93 and 0.91 for PBDT-2TC:4TBA:ITIC and PBDT-2TC:4TBA:4TIC, respectively, and significantly decreased to 0.88 for PBDT-2TC:4TBA:4TIC-4F, suggesting more charge recombination exist in these ternary blends. The recombination mechanisms in these devices can be further investigated according to the relationship of V_{oc} dependence on light intensity, as shown in **Fig. 5f**. The charge recombination process in blend films can be defined by the formula $V_{oc} \propto n(KBT/q)lnI$, where *KB*, *T* and *q* are the Boltzmann, absolute temperature and elementary charge, respectively.[57] A stronger dependence of V_{oc} on light intensity with a slope greater than *kT/q* is observed when the trap-assisted recombination is involved. In our cases, the dependence of V_{oc} on the light intensity for ternary devices based on two acceptors with different terminal's electronegativity were recorded with much higher slope than that based on two acceptors with the same terminal's dipole moment. The result also indicates that less trap-assisted recombination in these ternary devices based on combined acceptors with more compatible dipole moment. Therefore, the study of charge recombination mechanisms proved that the unbalanced charge transport which derived from the difference in the dipole moment of terminals between two acceptors could result in increased charge recombination, thus significantly decreasing the J_{sc} and FF in these ternary devices.

2.7. The Mechanism of Hypothesis

From the investigations of photophysical and photovoltaic properties, and the BHJ morphology, we have confirmed the influence of the dipole moment of acceptor's terminal groups in ternary OSCs. In two FREAs based ternary OSCs, the two acceptors with the same terminals invariably work well than that of the acceptors with different terminals. Based on these results, the compatible dipole moment seems to dominate the performance of the ternary blends, thus a schematic diagram of such working principle is proposed and presented in **Fig. 6**. If the terminals in two FREAs in the ternary blends have huge difference in electron-withdrawing ability, it would result in unbalanced charge transport, leading to increased charge combination in ternary OSCs. Consequently, the performance of the devices will significantly decrease in spite of adding only a small amount of the third component. On the contrary, if the two FREAs in the ternary blends possess different fused-rings but the same terminals, the blends exhibit more balanced charge transport and less charge recombination. Under the circumstances, the two FREAs with high compatibility result in better device performance.

To further verify the hypothesis, additional DFT calculation analysis was performed. It is well known that the strong π-π stacking between conjugated organic molecules can facilitate charge transport, thereby improving the performance of OSCs, and the π-π stacking is responsible by the dimer configurations[58]. The plots of electron density ρ(r) multiplied by the sign of the second Hessian eigenvalue λ_2 versus reduced density gradient (RDG) ($\boldsymbol{RDG} = \frac{\mathbf{1}}{\mathbf{2(3\pi^2)^{1/3}\rho^{4/3}}}|\nabla\boldsymbol{\rho}|$) for the dimers of six systems (4TBA:6TBA, 4TBA:ITIC, 4TBA:4TIC, 4TBA:4TIC-4F, 4TBA:STBA and 4TIC:ITIC) were created to understand the interaction nature for different stacking modes in **Fig.S9** and **Fig.7**. The blue, green and red areas in **Fig.7** stand for hydrogen bonds, Van der Waals interactions and steric repulsion, respectively[59]. The lowest energy dimer structures were obtained by Molclus program[60] and Gaussian. Additionally, RDG analysis of the terminal stacking regions between the acceptor molecules was performed by the Multiwfn software[61]. The π-π stacking interactions with a value of sign(λ_2)ρ around zero between the acceptor molecules' terminals are clearly manifested by the gradient isosurfaces (RDG = 0.5 a.u.). From the **Fig.S9** and **Fig.7**, it can be seen that the dimers (4TBA:6TBA, 4TBA:STBA, 4TIC:ITIC) with the same dipole moment terminals have better π-π interactions with more gradient isosurfaces. However, the gradient isosurface area between the 4TBA and 4TIC-4F terminals is the smallest, indicating that the dimers have the worst π-π interactions. The worst π-π stacking interaction in 4TBA:4TIC-4F blend may be detrimental to charge transfer and transport, which may explain why the PBDT-2TC:4TBA:4TIC-4F based device has significant unbalanced charge mobilities. These results indicate that the terminals' dipole moment of FREAs play an important role in ternary OSCs, which is consistent with our hypothesis.

3. Conclusions

In summary, a new important parameter of dipole moment is established in designing and evaluating the performance of ternary OSCs based on one conjugated polymer and two FREAs. Six ternary blends with complementary absorption and cascade energy levels were systematically constructed. From the results of studying these six ternary OSCs, we found that if there is a huge difference in two acceptors' terminal dipole moment, the electron mobility will be significantly decreased to result in unbalanced charge transport and more charge recombination, thus induce significant attenuated device performance. As a result, the PBDT-2TC:4TBA:6TBA blend shows the best performance while the PBDT-2TC:4TBA:4TIC-4F exhibits the worst performance even just adds a small amount of the third component 4TIC-4F. This is the first time that a comprehensive

study has been conducted to understand the role of dipole moment in affecting ternary OSCs. This method can be used as a rough guideline to screen ternary system for improving the device performance.

Conflicts of interest

There are no conflicts to declare.

Acknowledgements

X.L. thanks for the support from "the Fundamental Research Funds for the Central Universities" (2232019D3-04), Shanghai Sailing Program (19YF1401000), the National Natural Science Foundation of China (NSFC) (51973032, and 21905043), and the Initial Research Funds for Young Teachers of Donghua University. A.J. acknowledges the financial support from the Office of Naval Research (N00014-17-1-2201). Y.C. thanks for support from the National Natural Science Foundation of China (NSFC) (51673091, and 51833004). X-ray data was acquired at beamline 7.3.3 and 11.0.1.2 at Lawrence Berkeley National Laboratory, which is supported by the DOE, Office of Science, and Office of Basic Energy Sciences.

Author contributions

X.L and X.S. conceived the idea and designed the experiment with the help of L.C., L.Z, K.G. and F.L; X.L. performed the device fabrication and data analysis; Z.Y. and Y.C carried out the DFT simulation; Y.A. and Q.X. made the polymer PBDT-2CT that was not purchased; H.Z. and W.M. performed the GIWAXS characterization and data analysis; P.Z., Y.G. and X.F. help analysis the electrochemical measurements; X.L. wrote the original draft; All authors discussed the results and commented on the manuscript; Y.W.C. supervised the project.

Notes and references

1 Y. Lin, J. Wang, Z. G. Zhang, H. Bai, Y. F. Li, D. B. Zhu, X. Zhan. An Electron Acceptor Challenging Fullerenes for Efficient Polymer Solar Cells. *Adv. Mater*., 2015, **27**, 1170.

2 C. Yan, S. Barlow, Z. Wang, H. Yan, A. K.-Y. Jen, S. R. Marder, X. Zhan. Non-fullerene acceptors for organic solar cells. *Nat. Rev. Mater*., 2018, **3**, 18003.

3 S. Chen, H. Cho, J. Lee, Y. Yang, Z. Zhang, Y. Li, C. Yang. Modulating the Molecular Packing and Nanophase Blending via a Random Terpolymerization Strategy toward 11% Efficiency Nonfullerene Polymer Solar Cells. *Adv. Energy Mater*., 2017, 1701125.

4 M. Jeong, S. Chen, S. Lee, Z. Wang, Y. Yang, Z. Zhang, C. Zhang, M. Xiao, Y. Li, C. Yang. Feasible D1-A-D2-A Random Copolymers for Simultaneous High-Performance Fullerene and Nonfullerene Solar Cells. *Adv. Energy Mater*., 2017, 1702166.

5 Y. Wang, Z. Peng, S. Xiao, J. Yang, H. Zhou, L. Huang, L. Sun, Y. Zhou, L. Tan, Y. Chen. Highly stable Al-doped ZnO by ligand-free synthesis as general thickness-insensitive interlayers for organic solar cells. *Sci. China. Chem*., 2018, **61**, 127.

6 X. Xu, Z. Bi, W. Ma, Z. Wang, W.C.H. Choy, W. Wu, G. Zhang, Y. Li, Q. Peng. Highly efficient ternary-blend polymer solar cells enabled by a nonfullerene acceptor and two polymer donors with a broad composition tolerance. *Adv. Mater*., 2017, **29**, 1704271.

7 Y. Zhang, L. Shi, Y, Chen. Overview and Outlook of Random Copolymerization Strategy for Designing Polymer Solar Cells. *Acta Polym. Sin*., 2019, **50**, 13.

8 S. Li, L. Ye, W. Zhao, H. Yan, B. Yang, D. Liu, W. Li, H. Ade, J. Hou. A wide band gap polymer with a deep highest occupied molecular orbital level enables 14.2% efficiency in polymer solar cells. *J. Am. Chem. Soc*., 2018, **140**, 7159.

9 D. Liu, J. Wang, C. Gu, Y. Li, X. Bao, R. Yang. Stirring Up Acceptor Phase and Controlling Morphology via Choosing Appropriate Rigid Aryl Rings as Lever Arms in Symmetry-Breaking Benzodithiophene for High-Performance Fullerene and Fullerene-Free Polymer Solar Cell. *Adv. Mater*., 2018, 1705870.

10 Y. Yang, Z. Zhang, H. Bin, S. Chen, L. Xue, C. Yang, Y. Li. Side-chain isomerization on an n-type organic semiconductor ITIC acceptor makes 11.77% high efficiency polymer solar cells. *J. Am. Chem. Soc*., 2016, **138**, 15011.

11 F. Zhao, S. Dai, Y. Wu, Q. Zhang, J. Wang, L. Jiang, Q. Ling, Z. Wei, W. Ma, W. You, C. Wang, X. Zhan. Single-junction binary-blend nonfullerene polymer solar cells with 12.1% efficiency. *Adv Mater*., 2017, **29**, 1700144.

12 H. Yao, Y. Cui, R. Yu, B. Gao, H. Zhang, J. Hou. Design, synthesis, and photovoltaic characterization of a small molecular acceptor with an ultra-narrow band gap. *Angew. Chem., Int. Ed*., 2017, **56**, 3045.

13 C. Huang, X. Liao, K. Gao, L. Zuo, F. Lin, X. Shi, C.-Z. Li, F. Liu, Y. Chen, H. Chen, A. K.-Y. Jen. Highly efficient organic solar cells based on S, N-heteroacene non-fullerene acceptors. *Chem. Mater*., 2018, **30**, 5429.

14 J. Sun, X. Ma, Z. Zhang, J. Yu, J. Zhou, X. Yin, L. Yang, R. Geng, R. Zhu, F. Zhang, W. Tang. Dithieno[3,2-b:2',3'-d]pyrrol Fused Nonfullerene Acceptors Enabling Over 13% Efficiency for Organic Solar Cells. *Adv. Mater*., 2018, 1707150.

15 Z. Yao, X. Liao, K. Gao, F. Lin, X. Xu, X. Shi, L. Zuo, F. Liu, Y. Chen, A. K.-Y. Jen. Dithienopicenocarbazole-based acceptors for efficient organic solar cells with optoelectronic response over 1000 nm and an extremely low energy loss. *J. Am. Chem. Soc*., 2018, **140**, 2054.

16 Z. Xiao, X. Jia, L. Ding. Ternary organic solar cells offer 14% power conversion efficiency. *Sci. Bull*., 2017, **62**, 1562.

17 J. Yuan, Y. Zhang, L. Zhou, G. Zhang, H. Yip, T. Lau, X. Lu, C. Zhu, H. Peng, P. Johnson, et al. Single-junction organic solar cell with over 15% efficiency using fused-ring acceptor with electron-deficient core. *Joule*, 2019, **3**, 1140.

18 X. Shi, L. Zuo, S. Jo, K. Gao, F. Lin, F. Liu, A. K.-Y. Jen. Design of a highly crystalline low-band gap fused-ring electron acceptor for high-efficiency solar cells with low energy loss. *Chem. Mater*., 2017, **29**, 8369.

19 J. Zhang, H. S. Tan, X. Guo, A. Facchetti, H. Yan. Material insights and challenges for non-fullerene organic solar cells based on small molecular acceptors. *Nat. Energy,* 2018, **3**, 720.

20 Y. Cui, H. Yao, B. Gao, Y. Qin, S. Zhang, B. Yang, C. He, B. Xu, J. Hou. Fine-tuned photoactive and interconnection layers for achieving over 13% efficiency in a fullerene-free tandem organic solar cell. *J. Am. Chem. Soc*., 2017, **139**, 7302.

21 W. Li, A. Furlan, K. H. Hendriks, M. M. Wienk, R. A. J. Janssen. Efficient tandem and triple-junction polymer solar cells. *J. Am. Chem. Soc*., 2013, **135**, 5529.

22 F. Chen, J. Xu, Z. Liu, M. Chen, R. Xia, Y. Yang, T. K. Lau, Y. Zhang, X. Lu, H. L. Yip, A. K. Jen, H. Chen, C. Li. Near-Infrared Electron Acceptors with Fluorinated Regioisomeric Backbone

for Highly Efficient Polymer Solar Cells. *Adv. Mater*., 2018, **30**, 1803769.
23 Y. Li, J. D. Lin, X. Liu, Y. Qu, F. P. Wu, F. Liu, Z. Q. Jiang, S. R. Forrest. Near-Infrared Ternary Tandem Solar Cells. *Adv. Mater*., 2018, **30**, 1804416.
24 L. Zuo, X. Shi, S. B. Jo, Y. Liu, F. Lin, A. K. Jen. Tackling energy loss for high-efficiency organic solar cells with integrated multiple strategies. *Adv. Mater*., 2018, **30**, 1706816.
25 L. Meng, Y. Zhang, X. Wan, C. Li, X. Zhang, Y. Wang, X. Ke, Z. Xiao, L. Ding, R. Xia, H.-L. Yip, Y. Cao, Y. Chen. Organic and solution-processed tandem solar cells with 17.3% efficiency. *Science*, 2018, **361**, 1094.
26 Y. Yang, W. Chen, L. T. Dou, W. H. Chang, H. S. Duan, B. Bob, G. Li, Y. Yang. High-performance multiple-donor bulk heterojunction solar cells. *Nat. Photonics*, 2015, **9**, 190.
27 N. Gasparini, L. Lucera, M. Salvador, M. Prosa, G. D. Spyropoulos, P. Kubis, H.-J. Egelhaaf, C. J. Brabec, T. Ameri. High-performance ternary organic solar cells with thick active layer exceeding 11% efficiency. *Energy Environ. Sci*., 2017, **10**, 885.
28 L. Y. Lu, M. A. Kelly, W. You, L. P. Yu. Status and prospects for ternary organic photovoltaics. *Nat. Photonics*, 2015, **9**, 491.
29 X. Liao, J. Wang, S. Chen, L. Chen, Y. Chen. Diketopyrrolopyrrole-based conjugated polymers as additives to optimize morphology for polymer solar cells. *Chin. J. Polym. Sci*., 2016, **34**, 491.
30 D. Baran, T. Kirchartz, S. Wheeler, S. Dimitrov, M. Abdelsamie, J. Gorman, R. S. Ashraf, S. Holliday, A. Wadsworth, N. Gasparini, P. Kaienburg, H. Yan, A. Amassian, C. J. Brabec, J. R. Durrant, I. McCulloch. Reduced voltage losses yield 10% efficient fullerene free organ-ic solar cells with> 1 V open circuit voltages. *Energy Environ. Sci*., 2016, **9**, 3783.
31 W. Li, L. Yang, J. R. Tumbleston, L. Yan, H. Ade, W. You. Controlling Molecular Weight of a High Efficiency Donor-Acceptor Conjugated Polymer and Understanding Its Significant Impact on Photovoltaic Properties. *Adv. Mater*., 2014, **26**, 4456.
32 B. A. Collins, Z. Li, J. R. Tumbleston, E. Gann, C. R. McNeill, H. Ade. Absolute Measurement of Domain Composition and Nanoscale Size Distribution Explains Performance in PTB7:$PC_{71}BM$ Solar Cells. *Adv. Energy Mater*., 2013, **3**, 65.
33 H. Zhou, L. Yang, W. You. Rational design of high performance conjugated polymers for organic solar cells. *Macromolecules*, 2012, **45**, 607.
34 K. Jiang, G. Zhang, G. Yang, J. Zhang, Z. Li, T. Ma, H. Hu, W. Ma, H. Ade, H. Yan. Multiple Cases of Efficient Nonfullerene Ternary Organic Solar Cells Enabled by an Effective Morphology Control Method. *Adv. Energy Mater*., 2017, 1701370.
35 M. Zhang, W. Gao, F. J. Zhang, Y. Mi, W. B. Wang, Q. S. An, J. Wang, X. L. Ma, J. L. Miao, Z. H. Hu, X. F. Liu, J. Zhang, C. L. Yang. Efficient ternary non-fullerene polymer solar cells with PCE of 11.92% and FF of 76.5%. *Energy Environ. Sci*., 2018, **11**, 841.
36 Z. H. Luo, H. J. Bin, T. Liu, Z. G. Zhang, Y. K. Yang, C. Zhong, B. B. Qiu, G. H. Li, W. Gao, D. J. Xie, K. L. Wu, Y. M. Sun, F. Liu, Y. F. Li, C. L. Yang. Fine-Tuning of Molecular Packing and Energy Level through Methyl Substitution Enabling Excellent Small Molecule Acceptors for Nonfullerene Polymer Solar Cells with Efficiency up to 12.54%. *Adv. Mater*., 2018, **30**, 1706124.
37 Q. An, J. Zhang, W. Gao, F. Qi, M. Zhang, X. Ma, C. Yang, L. Huo, and F. Zhang. Efficient Ternary Organic Solar Cells with Two Compatible Non-Fullerene Materials as One Alloyed Acceptor. *Small*, 2018, **14**, 1802983.
38 J. Lee, S. J. Ko, M. Seifrid, H. Lee, C. McDowell, B. R. Luginbuhl, A. Karki, K. Cho, T. Q. Nguyen, and G. C. Bazan. Design of Nonfullerene Acceptors with Near-Infrared Light Absorption Capabilities. *Adv. Energy Mater*., 2018, *8*, 1801209.
39 X. L. Ma, W. Gao, J. S. Yu, Q. S. An, M. Zhang, Z. H. Hu, J. X. Wang, W. H. Tang, C. L. Yang, and F. J. Zhang. Ternary nonfullerene polymer solar cells with efficiency> 13.7% by integrating the advantages of the materials and two binary cells. *Energy Environ. Sci*., 2018, **11**, 2134.
40 H. Zhang, H. F. Yao, J. X. Hou, J. Zhu, J. Q. Zhang, W. N. Li, R. N. Yu, B. W. Gao, S. Q. Zhang, and J. H. Hou. Over 14% efficiency in organic solar cells enabled by chlorinated nonfullerene small-molecule acceptors. *Adv. Mater*., 2018, **30**, 1800613.
41 Q. An, J. Wang, W. Gao, X. Ma, Z. Hu, J. Gao, C. Xu, M. Hao, X. Zhang, C. Yang, F. Zhang. Alloy-like ternary polymer solar cells with over 17.2% efficiency. *Sci. Bull*., 2020, DOI: 10.1016/j.scib.2020.01.012.
42 T. Yan, W. Song, J. Huang, R. Peng, L. Huang, Z. Ge. 16.67% Rigid and 14.06% Flexible Organic Solar Cells Enabled by Ternary Heterojunction Strategy. *Adv. Mater*., 2019, 1902210.
43 M. Pan, T. Lau, Y. Tang, Y. Wu, T. Liu, K. Li, M. M. Chen, X. Lu, W. Ma and C. Zhan. 16.7%-efficiency ternary blended organic photovoltaic cells with PCBM as the acceptor additive to increase the open-circuit voltage and phase purity. *J. Mater. Chem. A*, 2019, **7**, 20713.
44 L. Zhan, S. Li, T. Lau, Y. Cui, X. Lu, M. Shi, C. Li, H. Li, J. Hou, H. Chen. Over 17% efficiency ternary organic solar cells enabled by two non-fullerene acceptors working in alloy-like model. *Energy Environ. Sci.,* 2020,**13**, 635.
45 Z. Zheng, O. Awartani, B. Gautam, D. Liu, Y. Qin, W. Li, A. Bataller, K. Gundogdu, H. Ade, J. Hou. Efficient charge transfer and fine-tuned energy level alignment in a THF-processed fullerene-free organic solar cell with 11.3% efficiency. *Adv. Mater*., 2017, **29**, 1604241.
46 M. Li, Y. Zhou, J. Zhang, J. Song, Z. Bo. Tuning the dipole moments of nonfullerene acceptors with an asymmetric terminal strategy for highly efficient organic solar cells. *J. Mater. Chem. A*, 2019, **7**, 8889.
47 Y. An, X. Liao, L. Chen, J. Yin, Q. Ai, Q. Xie, B. Huang, F. Liu, A. K.-Y. Jen, Y. Chen. Nonhalogen Solvent-Processed Asymmetric Wide-Bandgap Polymers for Nonfullerene Organic Solar Cells with Over 10% Efficiency. *Adv. Funct. Mater*., 2018, **28**, 1706517.
48 L. Zuo, X. Shi, S. Jo, Y. Liu, F. Lin, A. K.-Y. Jen. Tackling energy loss for high-efficiency organic solar cells with integrated multiple strategies. *Adv. Mater*., 2018, **30**, 1706816.
49 X. Shi, X. Liao, K. Gao, L. Zuo, J. Chen, J. Zhao, F. Liu, Y. Chen, A. K.-Y. Jen. An Electron Acceptor with Broad Visible-NIR Absorption and Unique Solid State Packing for As-Cast High Performance Bi-nary Organic Solar Cells. *Adv. Funct. Mater*., 2018, **28**, 1802324.
50 C.-Z. Li, C.-C. Chueh, H.-L. Yip, K. M. O'Malley, W.-C. Chen, A. K.-Y. Jen. Effective interfacial layer to enhance efficiency of polymer solar cells via solution-processed fullerene-surfactants. *J. Mater. Chem*., 2012, **22**, 8574.
51 A. Hexemer, W. Bras, J. Glossinger, E. Schaible, E. Gann, R. Kirian, A. MacDowell, M. Church, B. Rude, H. Padmore. A SAXS/WAXS/GISAXS beamline with multilayer monochromator. *J. Phys. Conf. Ser*., 2010, **247**, 012007.
52 L. Zhang, B. Lin, B. Hu, X. Xu and W. Ma. Blade-Cast Nonfullerene Organic Solar Cells in Air with Excellent Morphology, Efficiency, and Stability. *Adv. Mater*., 2018, **30**, 1800343.
53 L. Zhang, X. Xu, B. Lin, H. Zhao, T. Li, J. Xin, Z. Bi, G. Qiu, S. Guo, K. Zhou, X. Zhan, W. Ma. Achieving Balanced Crystallinity of Donor and Acceptor by Combining Blade-Coating and Ternary Strategies in Organic Solar Cells. *Adv. Mater*., 2018, **30**, 1805041.
54 V. Mihailetchi, J. Wildeman, P. Blom. Space-charge limited photocurrent. *Phys. Rev. Lett*., 2005, **94**, 126602.
55 A. K. K. Kyaw, D. H. Wang, V. Gupta, W. L. Leong, L. Ke, G. C. Bazan, A. J. Heeger. Intensity dependence of current-voltage

characteristics and recombination in high-efficiency solution-processed small-molecule solar cells. *ACS Nano*, 2013, **7**, 4569.

56 R. Ingo, P. Jürgen, D. Vladimir, L. Laurence, V. Dirk, C. H. Jan. Effect of Temperature and Illumination on the Electrical Characteristics of Polymer-Fullerene Bulk-Heterojunction Solar Cells. *Adv. Funct. Mater*., 2004, **14**, 38.

57 L. J. A. Koster, V. D. Mihailetchi, R. Ramaker, P. W. M. Blom. Light intensity dependence of open-circuit voltage of polymer: fullerene solar cells. *Appl. Phys. Lett*., 2005, **86**, 1235.

58 G. Han, Y. Yi and Z. Shuai. From molecular packing structures to electronic processes: theoretical simulations for organic solar cells. *Adv. Energy Mater.*, 2018, **8**, 1702743.

59 E. R. Johnson, S. Keinan, P. Mori-Sa´nchez, J. Contreras-Garcıa, A. J. Cohen and W. Yang. Revealing noncovalent interactions. *J. Am. Chem. Soc.*, 2010, **132**, 6498.

60 T. Lu. Molclus Program, Version 1.9, http://www.keinsci.com/research/molclus.html.

61 T. Lu, F. Chen. Multiwfn: a multifunctional wavefunction analyser. *J. Comput. Chem.*, 2012, **33**, 580.

ARTICLE

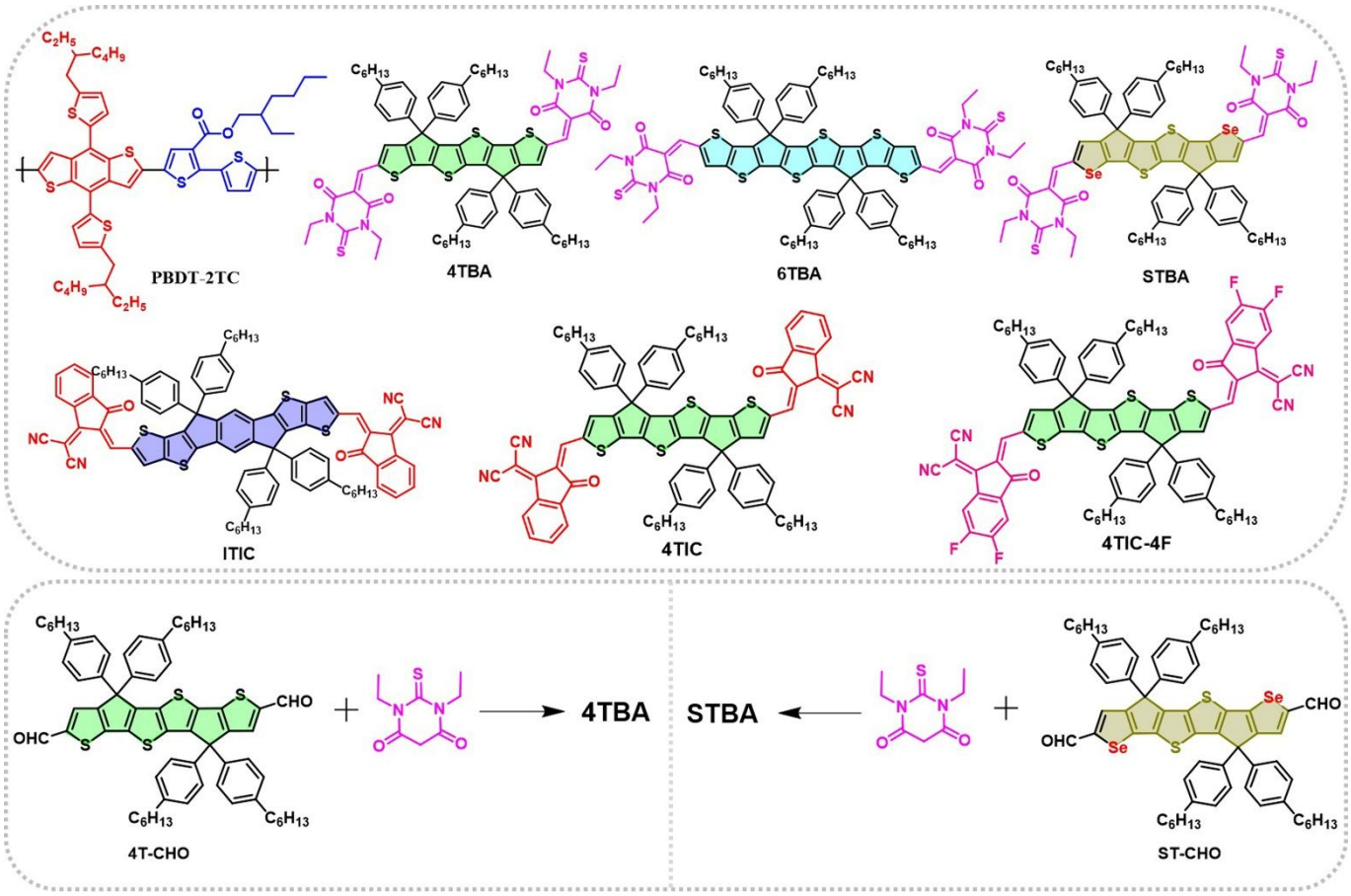

Scheme 1. (a) Molecular structures of the polymer donor PBDT-2TC and non-fullerene acceptors 4TBA, 6TBA, STBA, ITIC, 4TIC and 4TIC-4F. (b) The synthetic routes of 4TBA and STBA.

ARTICLE

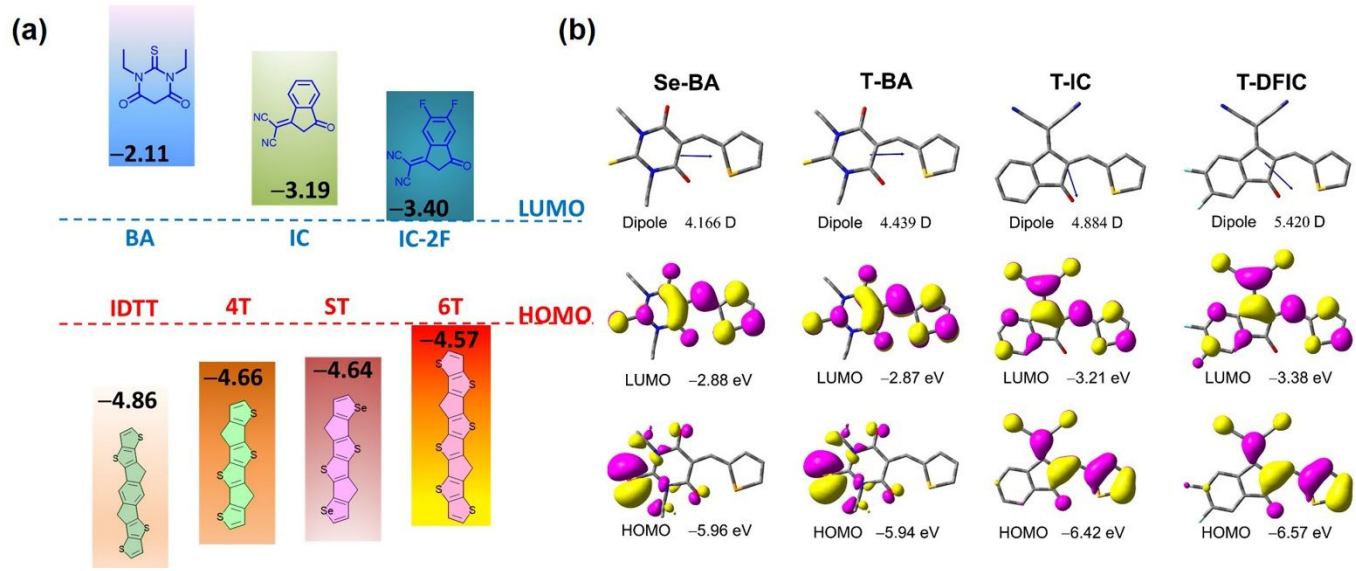

Fig. 1 (a) Energy levels of cores and end groups calculated by DFT. (b) Dipole moments for the regional parts (Se-BA, T-BA, T-IC, T-FIC and T-DFIC) in the asymmetric molecules.

ARTICLE

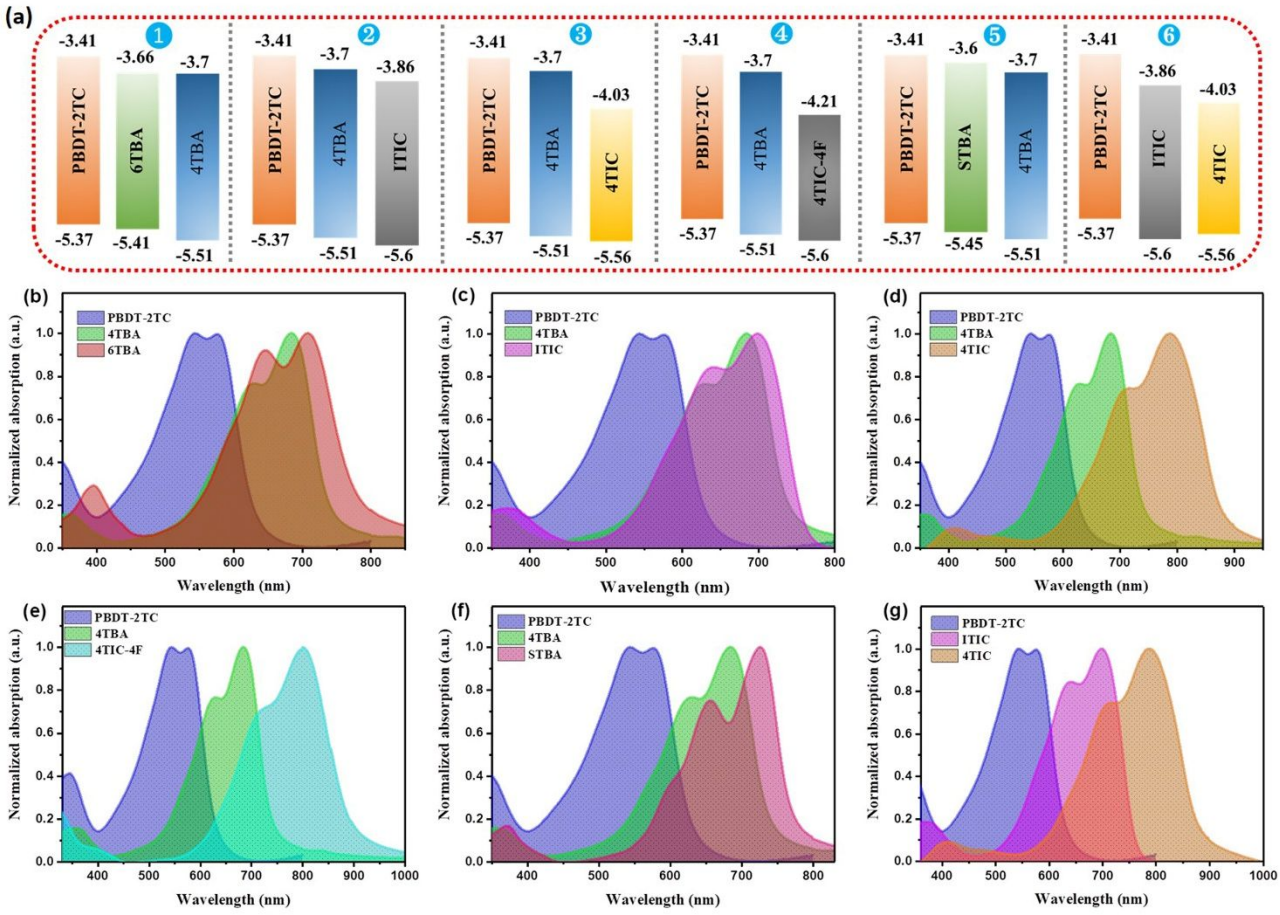

Fig. 2 (a) Energy diagrams of six ternary systems' materials. (b-f) Normalized UV–vis absorption spectra for the materials of six ternary blends.

ARTICLE

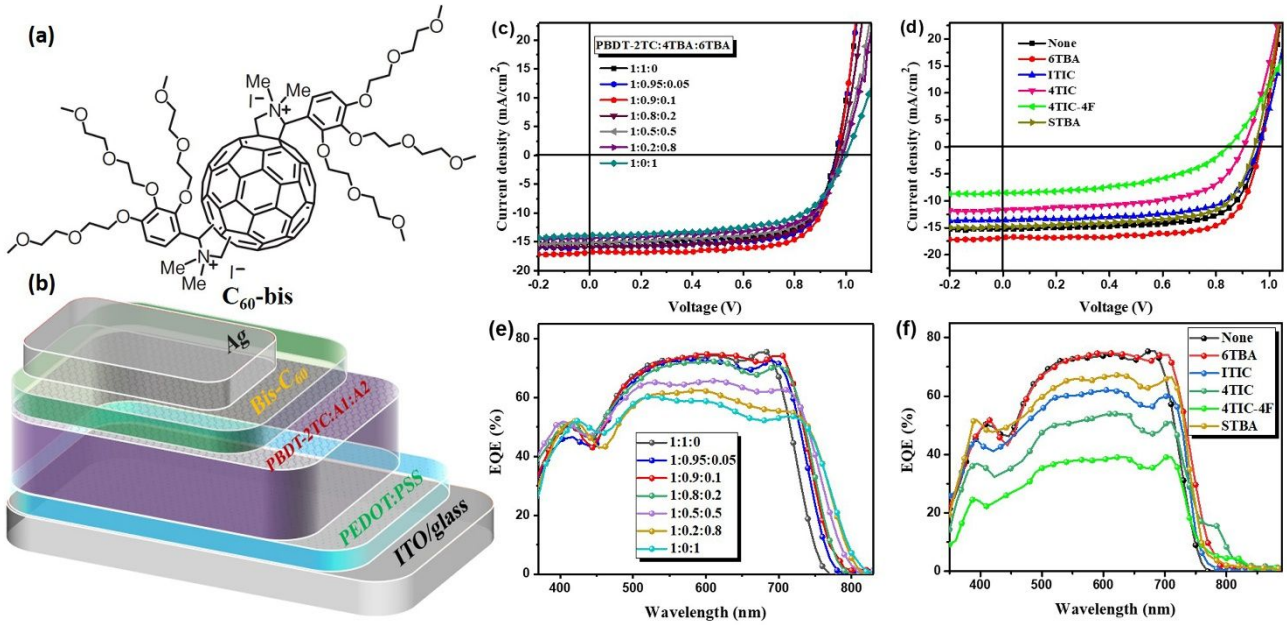

Fig. 3 (a) Molecular structure of C_{60}-bis. (b) Device architecture. (c) *J*–*V* curves of PBDT-2TC:4TBA:6TBA based OSCs with different acceptor contents. (d) *J*–*V* curves of multiple ternary systems based OSCs (PBDT-2TC:4TBA:Acceptor 2 = 1:0.9:0.1). (e-f) EQE spectra of the respective ternary devices.

ARTICLE

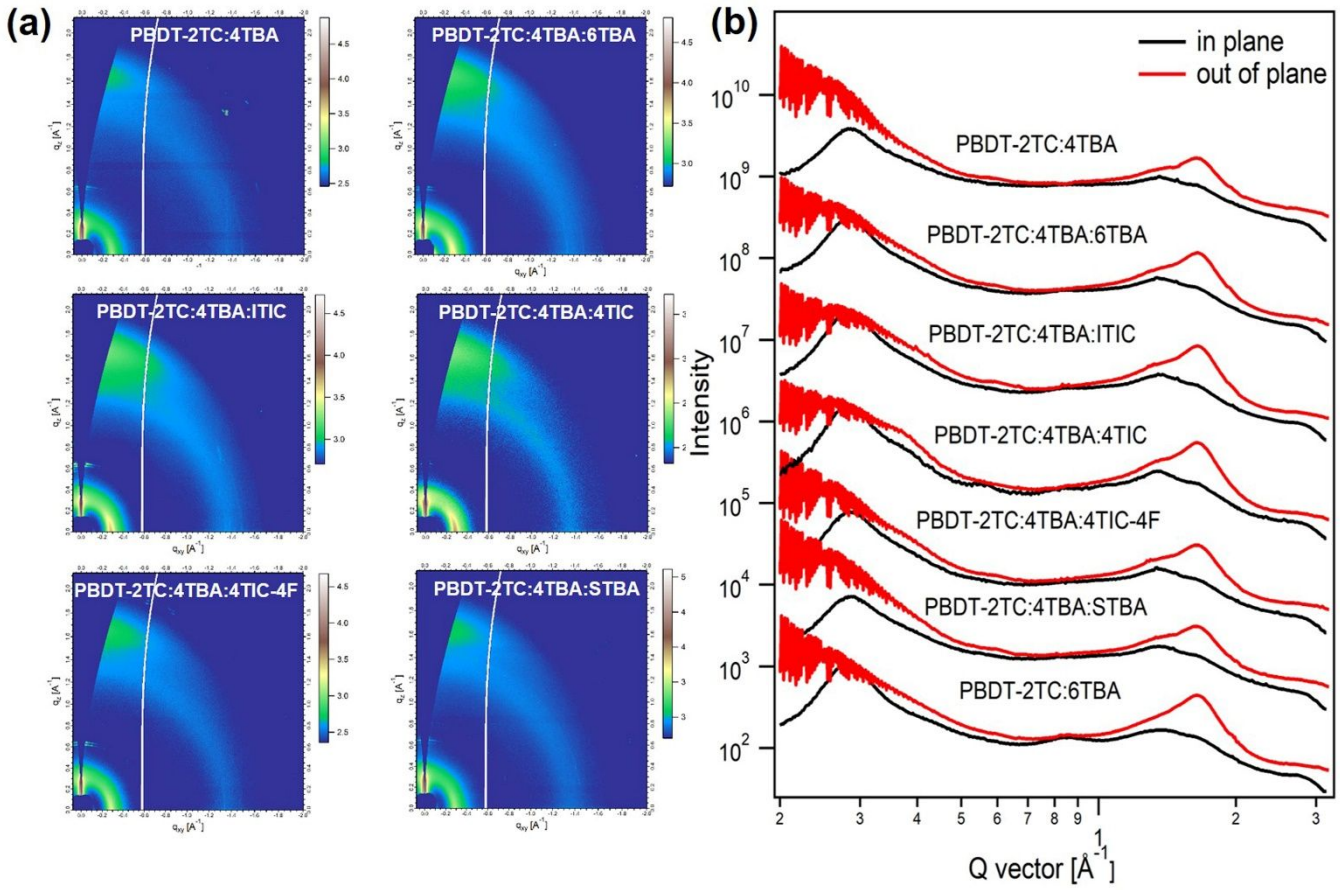

Fig. 4 (a) 2D GIWAXS patterns for PBDT-2TC:4TBA, PBDT-2TC:4TBA:6TBA, PBDT-2TC:4TBA:ITIC, PBDT-2TC:4TBA:4TIC, PBDT-2TC:4TBA:4TIC-4F, PBDT-2TC:4TBA:STBA. (b) In-plane (black line) and out-of-plane (red line) line-cut profiles of GIWAXS results.

ARTICLE

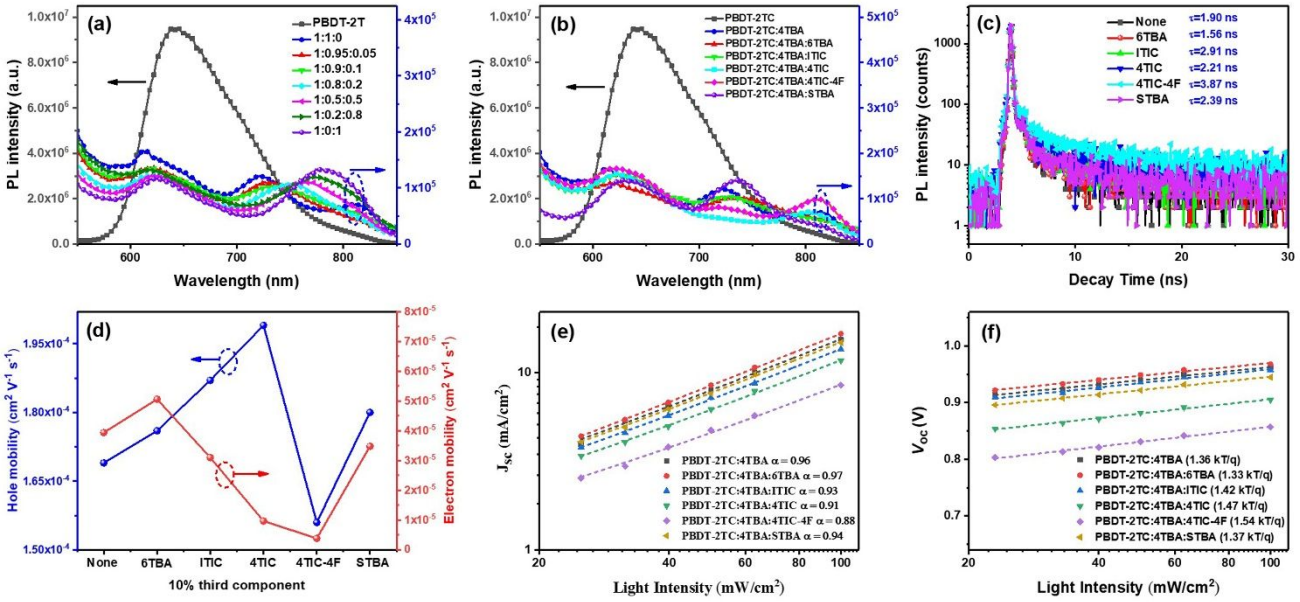

Fig. 5 (a) PL spectra of the pristine polymer film and active blend films with different weight ratios of 4TBA:6TBA. (b) PL spectra of the pristine polymer film and PBDT-2TC:4TBA blended films with or without different third acceptor component (10wt%). (c) TRPL spectra of PBDT-2TC:4TBA blended films with or without different third acceptor component (10wt%). (d) hole mobility and electron mobility dependence on 10wt% third component. Light intensity dependence of (e) J_{sc} and (f) V_{oc} of the blended films with or without different third acceptor component based devices.

ARTICLE

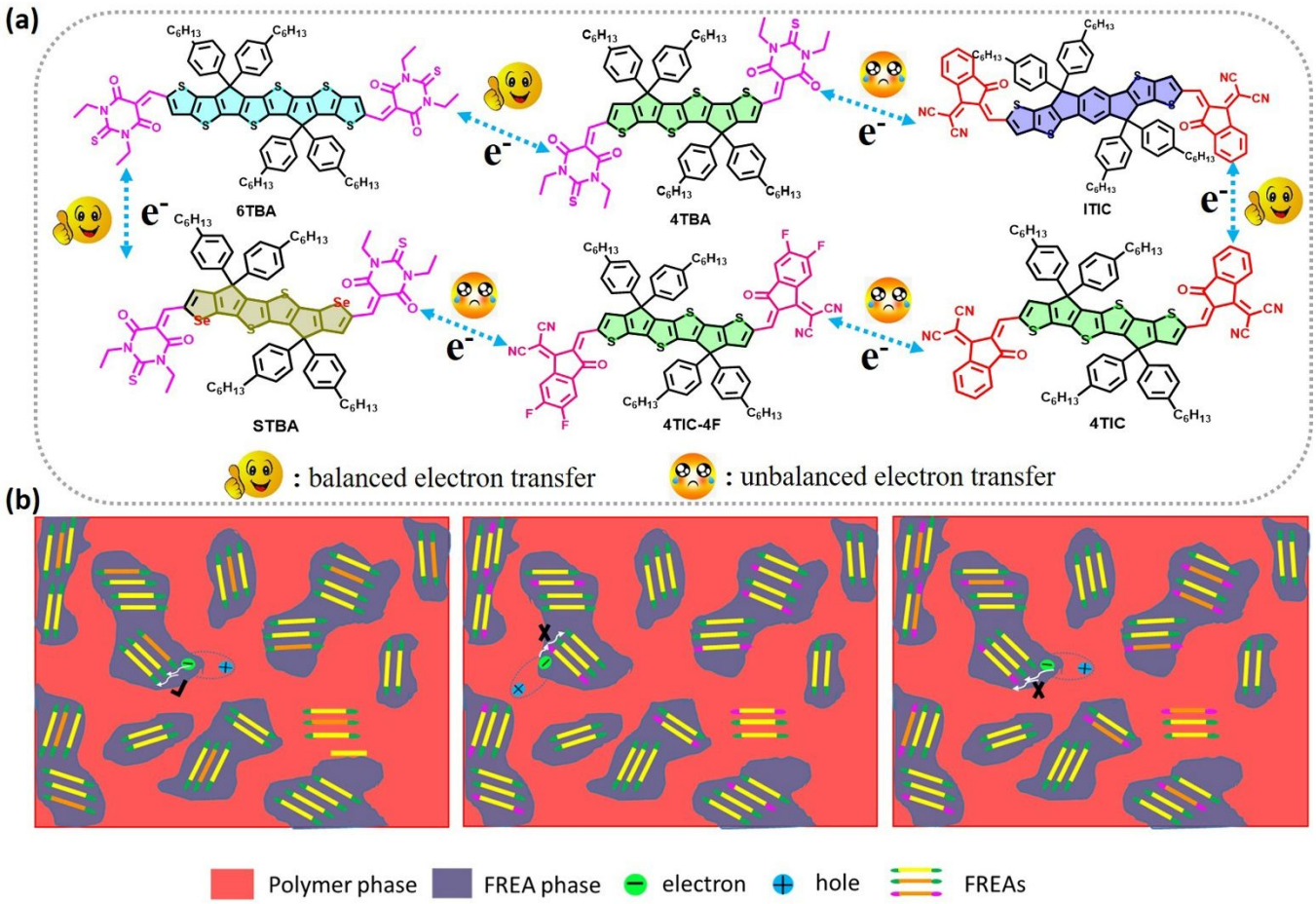

Fig. 6 (a) Hypothetical mechanism diagram of electron transport in ternary blends reflected by molecular structures. (b) The possible charge transport pathway existing in three different type ternary systems, the yellow and orange segments in FREAs represent the donor cores, the green and pink segments represent terminals and different colors represent different donor core or terminals.

ARTICLE

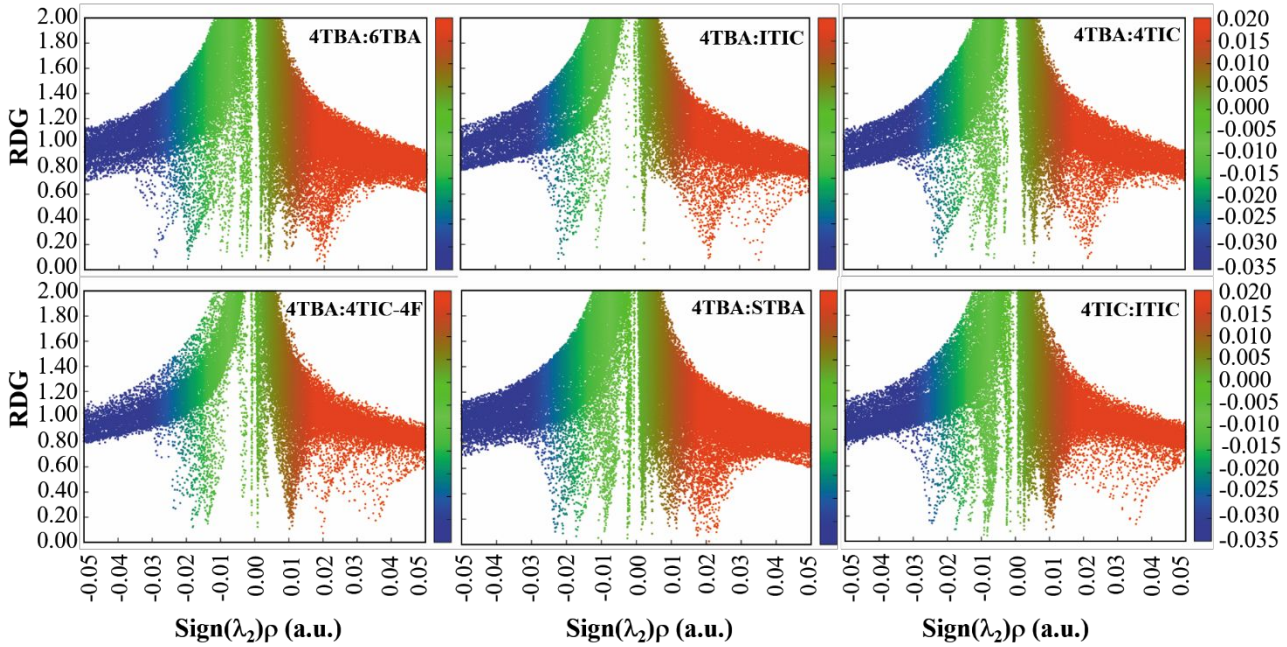

Fig.7 The plots of the production of electron density ρ(r) and the sign of the second Hessian eigenvalue λ_2 versus RDG for six combinations of 4TBA:6TBA, 4TBA:ITIC, 4TBA:4TIC, 4TBA:4TIC-4F, 4TBA:STBA and 4TIC:ITIC.

ARTICLE

Table 1. Photovoltaic parameter of OSCs based on ternary blends.

Active layer	D/A ratio	V_{OC} (V)	J_{SC} (mA/cm^2)	FF	PCE (%)[a]	Calc. *J*sc (mA/cm^2)
PBDT-2TC:4TBA:6TBA	1:1:0	0.962 (0.960 ± 0.004)	15.4 (15.2 ± 0.3)	0.71 (0.70 ± 0.01)	10.52 (10.13 ± 0.28)	14.9
	1:0.95:0.05	0.965 (0.964 ± 0.003)	15.8 (15.6 ± 0.4)	0.72 (0.71 ± 0.02)	10.98 (10.56 ± 0.32)	15.2
	1:0.9:0.1	**0.968 (0.966 ± 0.004)**	**16.6 (16.4 ± 0.4)**	**0.73 (0.71 ± 0.02)**	**11.73 (11.25 ± 0.38)**	**16.1**
	1:0.8:0.2	0.972 (0.970 ± 0.005)	15.7 (15.5 ± 0.3)	0.69 (0.78 ± 0.02)	10.53 (10.15 ± 0.27)	15.2
	1:0.5:0.5	0.981 (0.979 ± 0.004)	15.2 (14.9 ± 0.4)	0.66 (0.65 ± 0.02)	9.84 (9.44 ± 0.31)	14.7
	1:0.2:0.8	0.988 (0.986 ± 0.005)	14.4 (14.2 ± 0.3)	0.65 (0.64 ± 0.02)	9.25 (8.98 ± 0.25)	13.9
	1::0:1	1.0 (0.998 ± 0.004)	13.9 (13.8 ± 0.3)	0.63 (0.62 ± 0.02)	8.76 (8.46 ± 0.27)	13.6
PBDT-2TC:4TBA:ITIC	1:0.9:0.1	0.958 (0.957 ± 0.003)	13.6 (13.4 ± 0.3)	0.67 (0.66 ± 0.02)	8.73 (8.41 ± 0.25)	13.2
PBDT-2TC:4TBA:4TIC	1:0.9:0.1	0.905 (0.903 ± 0.005)	11.7 (11.5 ± 0.4)	0.60 (0.59 ± 0.01)	6.35 (6.07 ± 0.21)	11.3
PBDT-2TC:4TBA:4TIC-4F	**1:0.9:0.1**	**0.857 (0.854 ± 0.006)**	**8.5 (8.3 ± 0.3)**	**0.49 (0.48 ± 0.02)**	**3.57 (3.29 ± 0.18)**	**8.2**
PBDT-2TC:4TBA:STBA	1:0.9:0.1	0.945 (0.943 ± 0.004)	14.8 (14.5 ± 0.4)	0.68 (0.67 ± 0.02)	9.51 (9.23 ± 0.25)	14.3
PBDT-2TC:ITIC:4TIC	**1:0.9:0.1**	**0.893 (0.892 ± 0.003)**	**17.3 (17.0 ± 0.5)**	**0.70 (0.68 ± 0.02)**	**10.81 (10.42 ± 0.33)**	**16.7**
PBDT-2TC:ITIC	1:1	0.939 (0.937 ± 0.003)	15.8 (15.6 ± 0.4)	0.67 (0.66 ± 0.02)	9.94 (9.56 ± 0.28)	15.3

[a]Average values obtained from ten devices are shown in parentheses.

Table 2. The Parameters of Hole and Electron Mobilities.

Active layer	u_h [10^{-4} cm^2 V^{-1} s^{-1}]	u_e [10^{-5} cm^2 V^{-1} s^{-1}]	u_h/u_e
PBDT-2TC:4TBA	1.69	3.94	4.23
PBDT-2TC:4TBA:6TBA	1.76	5.06	3.48
PBDT-2TC:4TBA:ITIC	1.87	3.10	6.03
PBDT-2TC:4TBA:4TIC	1.99	0.97	20.52
PBDT-2TC:4TBA:4TIC-4F	1.56	0.39	40
PBDT-2TC:4TBA:STBA	1.80	3.48	5.17

u_h: Hole mobility. **u_e:** Electron mobility. The balance of hole and electron mobilities (u_h/u_e).

ARTICLE

Graphical contents entry

A new considerable factor of the dipole moment of FREAs' terminals is unveiled and its working mechanism has been thoroughly investigated. Our results demonstrate that the dipole moment should also be taken into account in designing ternary OSCs.